Bayesian Prediction-Powered Inference: Conjugate Base Model and MCMC Extensions*

Anonymous authors
Paper under double-blind review

Abstract

Modern predictors trained on vast unlabeled corpora can be highly accurate yet systematically biased, complicating valid uncertainty quantification when only a small labeled set is available. Prediction–Powered Inference (PPI) addresses this by correcting an imputed estimator with a rectifier computed on labeled data, yielding frequentist guarantees under mild conditions. We develop a fully Bayesian analogue of PPI that (i) exploits the *conjugate* Beta–Bernoulli structure of the base chain-rule model to obtain posteriors for $(\theta_A, \theta_{H|1}, \theta_{H|0})$ in closed form and map draws directly to g, and (ii) uses NUTS/MCMC only when moving beyond conjugacy (e.g., hierarchical partial pooling, non-Beta priors via logit-normal parameterizations, K-bin generalizations, or joint inference over a threshold t). Implemented via direct sampling from the conjugate posteriors in the base case, and via the No–U–Turn Sampler (NUTS) in non-conjugate extensions, our Bayesian chain–rule estimator achieves near-nominal coverage with intervals that are typically shorter than (i) a labeled-only Bayesian baseline and (ii) a classical difference estimator, at matched label budgets.

Beyond CRE, we benchmark a *prior-free, analytic* PPI baseline that uses the autorater's continuous probabilities with small-sample t-critical values, and we introduce two deployment-facing audits: (a) labeled–unlabeled *exchangeability diagnostics* via propensity-overlap, and (b) *threshold uncertainty* control through out-of-fold (OOF) versus leaky selection and bootstrap dispersion of Youden's cutpoint. Synthetic studies and a medical–imaging case study on Alzheimer's disease MRI show label-efficiency gains while maintaining coverage, including age-aware operating points(with a fixed 65–70 analysis reported explicitly). All code and configuration to reproduce figures and tables are available at `(anonymizedlinkorOpenReviewartifactlink)`.

1 Introduction

Motivation. High–capacity machine–learning (ML) systems now achieve strong predictive performance in high–dimensional, nonparametric regimes. Translating these predictions into *valid statistical inference*—for example, interval estimates with nominal coverage—remains challenging when models are misspecified or over–parameterized and when human labels are scarce. Likelihood–based intervals may undercover or overcover in such regimes, whereas purely imputed estimators that replace outcomes by model predictions are typically biased. Related literatures on semi–supervised and survey–calibrated estimation show that auxiliary predictions can reduce variance if their bias is corrected appropriately (Lohr, 2019).

Prediction–Powered inference (PPI). PPI leverages an accurate but imperfect predictor trained on abundant unlabeled data and then debiases it using a small labeled subset via a *rectifier* term, yielding

*Code and scripts (anonymized) available at `(anonymizedlinkorOpenReviewartifactlink)`.

*Data used in preparation of this article were obtained from the Alzheimer's Disease Neuroimaging Initiative (ADNI) database (`adni.loni.usc.edu`). As such, the investigators within the ADNI contributed to the design and implementation of ADNI and/or provided data but did not participate in the analysis or writing of this report. A complete listing of ADNI investigators can be found at `http://adni.loni.usc.edu/wp-content/uploads/how_to_apply/ADNI_Acknowledgement_List.pdf`.

finite–sample guarantees under weak assumptions (Angelopoulos et al., 2023; Guo & Lei, 2021). For a binary autorater $A \in 0, 1$ and human label $H \in 0, 1$, the quantity of interest

$$g \;=\; P(H{=}1) \;=\; P(H{=}1 \mid A{=}1)P(A{=}1) + P(H{=}1 \mid A{=}0)P(A{=}0) \;=\; \theta_A\,\theta_{H|1} + (1-\theta_A)\,\theta_{H|0}, \qquad (1.1)$$

naturally couples plentiful predictions with few labels. In practice, the benefit of this coupling is largest when unlabeled predictions are abundant and labeling is costly—precisely the setting of modern applications in medical imaging and scientific data analysis. In addition to the thresholded-A formulation, we also consider a *continuous-probability* variant in which

$$\hat{g}_{\mathrm{PPI}} \;=\; \underbrace{\frac{1}{N}\sum_{i=1}^{N} p_i}_{\bar{p}} \;+\; \underbrace{\frac{1}{n}\sum_{i=1}^{n}(H_i - p_i)}_{\text{rectifier}}, \quad \mathrm{SE}(\hat{g}_{\mathrm{PPI}}) = \sqrt{\mathrm{Var}(p)/N + \mathrm{Var}(H-p)/n},$$

and we form 95% intervals with a normal critical value when $n \geq 30$ (otherwise $t_{0.975,n-1}$), yielding a *prior-free analytic* baseline complementary to our Bayesian approach (Angelopoulos et al., 2023; Efron & Tibshirani, 1993).

From conjugate Bayes to general Bayesian PPI. Recent Bayesian analyses of PPI provide closed forms in conjugate settings (e.g., beta–binomial or normal–linear), clarifying how rectifiers align with posterior predictive adjustments (Hofer et al., 2024). However, realistic applications often break conjugacy (e.g., hierarchical components, nuisance parameters, nonstandard likelihoods) and thus require simulation–based inference. In addition, domain deployment raises concerns about dataset shift between the unlabeled pool and the labeled subset, for which sensitivity analyses and stratification are recommended (Quiñonero-Candela et al., 2009; Moreno-Torres et al., 2012).

This paper: Bayesian PPI via conjugacy (base) and MCMC (extensions). We formulate a coherent Bayesian model for equation 1.1 with independent Beta priors on $(\theta_A, \theta_{H|1}, \theta_{H|0})$. In the base Beta–Bernoulli specification the posterior factorizes into independent Betas determined by simple cell counts, so uncertainty for $g = \theta_A\theta_{H|1} + (1-\theta_A)\theta_{H|0}$ follows by direct sampling. We then use Hamiltonian Monte Carlo (NUTS) only for realistic extensions that break conjugacy—logit-normal hierarchical pooling, non-Beta priors, K-bin score models, or joint inference over an operating threshold t— retaining a unified workflow and diagnostics (Neal, 2011; Betancourt, 2017; Hoffman & Gelman, 2014).

Contributions. Building on the PPI framework, we:

- exploit conjugacy in the base chain-rule model to obtain closed-form posteriors and direct uncertainty propagation to g;
- generalize beyond conjugacy with NUTS (hierarchical partial pooling, non-Beta priors via logit-normal, K-bin generalizations, joint threshold t), with clear posterior diagnostics (e.g., $\hat{R}$, ESS, divergences);
- introduce a *prior-free, analytic* PPI baseline that uses continuous autorater probabilities and t-critical values at small n for deployment-ready intervals (Angelopoulos et al., 2023; Efron & Tibshirani, 1993);
- add *deployment audits*: labeled–unlabeled *propensity-overlap* checks for exchangeability, and *OOF vs. leaky* threshold selection with bootstrap dispersion of Youden's cutpoint to avoid optimistic bias (Varma & Simon, 2006; Cawley & Talbot, 2010; Rosenbaum & Rubin, 1983; Youden, 1950);
- empirically compare the Bayesian chain–rule estimator (CRE) to a labeled–only Bayesian baseline and *two prior-free baselines*—the classical difference estimator (binary A) and the PPI estimator using probabilities p—in controlled simulations (bias/RMSE, interval width, coverage), while fixing the labeled indices across priors so that prior sensitivity is isolated to CRE/NB;
- demonstrate a medical–imaging case study (Alzheimer's disease MRI) that examines calibration and age–aware operating thresholds alongside coverage, including a fixed 65–70 subset analysis..

Empirical overview. Across synthetic experiments, CRE attains near-nominal coverage with narrower intervals than baselines at matched label budgets; effects attenuate when labeled strata are extremely small or severely imbalanced. In the MRI case study, CRE maintains calibrated uncertainty while enabling age–stratified operating points that improve accuracy or specificity without retraining the model. Because clinical deployment often depends on well–calibrated probabilities, we also analyze calibration and simple post–hoc fixes (e.g., temperature scaling), which preserve discrimination while improving reliability (Guo et al., 2017; Niculescu-Mizil & Caruana, 2005). In addition, the prior-free PPI baseline provides a transparent reference unaffected by Bayesian prior choice.

Limitations. Our analysis targets population–level functionals of the type in equation 1.1 under exchangeability of labeled and unlabeled samples. The method inherits sensitivity to severe dataset shift between the autorater pool and the labeled subset; we discuss diagnostics and mitigations (e.g., stratified labeling and prior sensitivity checks) (Quiñonero-Candela et al., 2009; Moreno-Torres et al., 2012). As with any MCMC approach, reliability depends on effective diagnostics and model adequacy (Betancourt, 2017). Finally, improperly selected thresholds (e.g., leaky reuse of evaluation data) can bias operating points; our OOF protocol and bootstrap dispersion address this risk (Varma & Simon, 2006; Cawley & Talbot, 2010).

Broader impact. Coupling abundant machine predictions with scarce labels can reduce annotation burdens in sensitive domains (e.g., medical imaging). At the same time, decision–threshold choices and calibration must be aligned with clinical costs and equity considerations; our age–aware analysis illustrates one such alignment while emphasizing the need for domain governance and prospective monitoring.

2 Background and Related Work

2.1 Prediction–Powered inference in context: links to survey calibration, semi–supervised inference, and doubly robust estimators

Prediction–Powered Inference (PPI) exploits a high–quality but imperfect predictor trained on abundant unlabeled samples to reduce variance at fixed label budgets while preserving valid uncertainty quantification. Let $\{(X_i, Y_i)\}_{i=1}^N$ be inputs and outcomes and let f be a predictor trained chiefly on unlabeled covariates. A purely imputed estimator $\hat{\theta}_f = N^{-1}\sum_i f(X_i)$ is generally biased, whereas the classical mean $\hat{\theta} * \text{classical} = N^{-1}\sum_i Y_i$ is label–hungry. PPI combines the strengths by introducing a rectifier on a small labeled subset $\{(X_i, Y_i)\}_{i=1}^N$ with $n \ll N$,

$$\Delta = \frac{1}{n}\sum_{i=1}^{n}\big(f(X_i) - Y_i\big), \qquad \hat{\theta}_{\text{PPI}} = \hat{\theta}_f - \Delta,$$

and provides finite–sample guarantees under weak assumptions on the sampling of the labeled subset and mild regularity of f (Angelopoulos et al., 2023; Guo & Lei, 2021). In binary–decision settings with a machine autorater $A \in 0, 1$ and a human label $H \in 0, 1$, the target positivity rate $g = P(H{=}1)$ decomposes via the chain rule

$$g = P(H{=}1 \mid A{=}1)P(A{=}1) + P(H{=}1 \mid A{=}0)P(A{=}0) = \theta_A\theta_{H|1} + (1-\theta_A)\theta_{H|0},$$

which exposes how abundant predictions (informing θ_A) and scarce labels (informing $\theta_{H|a}$) jointly determine uncertainty. The same structure underlies the *difference estimator*

$$\hat{g}_{\text{diff}} = \bar{A} + \overline{(H - A)} = \frac{1}{N}\sum_{i=1}^{N} A_i + \frac{1}{n}\sum_{i=1}^{n}(H_i - A_i),$$

long studied in design–based survey sampling where auxiliary variables reduce variance without sacrificing unbiasedness (Cochran, 1977; Lohr, 2019). From this perspective, PPI can be viewed as bringing classical calibration ideas to modern ML auxiliaries. The generalized regression (GREG) and calibration estimators (Särndal et al., 1992; Deville & Särndal, 1992) adjust sampling weights (or add regression corrections) so that estimates align with known population totals; replacing "known totals" by "accurate large–N machine predictions" recovers the spirit of PPI while retaining transparent conditions for coverage.

Connections to semi–supervised inference further clarify efficiency gains. A line of work on semi–supervised means, risks, and ROC–type functionals shows that plug–in estimators based on unlabeled X can be augmented by labeled residuals to attain substantial variance reduction with valid inference (Chakrabortty & Cai, 2018; Gronsbell & Cai, 2018). In influence–function language, the rectifier acts as an augmentation term that centers the estimating equation, a device familiar from augmented inverse–probability weighting and targeted learning where *doubly robust* estimators remain consistent if either the outcome or propensity/auxiliary model is correct (Bang & Robins, 2005; van der Laan & Rose, 2011). PPI differs in emphasis: assumptions are simple and practically auditable (exchangeability of labeled/unlabeled pools and predictor stability), and coverage statements leverage the large pool of machine predictions directly (Angelopoulos et al., 2023).

For practical deployment, we emphasize two additional ingredients often underplayed in prior narratives. First, when thresholds map scores to decisions ($A = \mathbf{1}S \geq t$), *leakage* can inflate performance if the same data inform threshold selection and evaluation; out-of-fold selection and bootstrap dispersion of Youden's cutpoint mitigate this bias (Youden, 1950; Varma & Simon, 2006; Cawley & Talbot, 2010; Efron & Tibshirani, 1993). Second, because PPI and CRE hinge on exchangeability between labeled and unlabeled pools, we advocate *propensity-overlap diagnostics* (e.g., low AUC for a labeled-versus-unlabeled classifier) as a simple precondition check (Rosenbaum & Rubin, 1983).

Practical deployment also requires calibrated probabilities when thresholding scores into $A = \mathbf{1}S \geq t$. Post–hoc calibration methods—Platt scaling (logistic/temperature scaling) and isotonic regression—improve probability reliability without changing ranking and therefore do not alter threshold–agnostic discrimination (AUC) (Platt, 1999; Zadrozny & Elkan, 2002; Niculescu-Mizil & Caruana, 2005; Guo et al., 2017). This integrates neatly with PPI: calibration sharpens decision quality, while the PPI estimator consumes only the thresholded A and labeled pairs to produce valid intervals for g. When labeled data are scarce or stratified (e.g., by age), information sharing through partial pooling or calibration across strata can stabilize estimates while respecting heterogeneity, as we adopt in the case study.

2.2 Bayesian formulations of PPI, computation, and diagnostics

A Bayesian treatment of PPI provides a coherent generative specification and direct uncertainty propagation to nonlinear functionals. In conjugate families (e.g., beta–binomial, normal–linear), recent work derives closed–form posteriors and clarifies how the PPI rectifier aligns with posterior predictive adjustments (Hofer et al., 2024). Realistic deployments often break conjugacy, especially when incorporating stratification, flexible priors, or additional structure. In these cases simulation–based inference via Hamiltonian Monte Carlo (HMC) and the No–U–Turn Sampler (NUTS) delivers efficient exploration with minimal tuning (Neal, 2011; Hoffman & Gelman, 2014; Betancourt, 2017).

In the base model with independent Beta priors and Bernoulli likelihoods for $(\theta_A, \theta_{H|1}, \theta_{H|0})$, conjugacy yields closed-form posteriors: each component is Beta with updated counts from $\mathcal{D}_A$ and the labeled 2×2 margins. Hence, one can obtain uncertainty for the functional g by drawing from these Betas and transforming. We resort to simulation-based inference (HMC/NUTS) when moving beyond conjugacy—e.g., with logit-normal hierarchies, non-Beta priors, K-bin generalizations with shared hyperparameters, or joint inference on t (Salvatier et al., 2016; Carpenter et al., 2017). Workflow discipline is crucial: rank–normalized $\hat{R} < 1.01$, adequate bulk/tail effective sample sizes (ESS), and the absence of divergences indicate reliable exploration; posterior–predictive checks (PPCs) and simulation–based calibration (SBC) ensure calibrated inferences for both primitive parameters and derived functionals like $g = \theta_A\theta_{H|1} + (1-\theta_A)\theta_{H|0}$ (Kumar et al., 2019; Vehtari et al., 2021b; Gabry et al., 2019; Talts et al., 2018; Vehtari et al., 2021a; McElreath, 2020).

Two modeling choices help in small–n or imbalanced strata. First, weakly informative priors (e.g., Jeffreys $\text{Beta}\left(\frac{1}{2}, \frac{1}{2}\right)$) regularize extreme cell proportions when labeled counts for A=1 or A=0 are tiny, improving tail behavior of credible intervals with minimal bias (Gelman et al., 2013). Second, hierarchical extensions with partial pooling across subgroups g share signal while preserving between–group differences; the induced group–wise estimands $g_g = \theta_{A,g}\theta_{H|1,g} + (1-\theta_{A,g})\theta_{H|0,g}$ inherit shrinkage–stabilized uncertainty. Model comparison within this family can be guided by PSIS–LOO expected log predictive density to avoid over–binning or over–stratification that does not improve out–of–sample fit (Vehtari et al., 2017).

Finally, distribution shift and label–missingness mechanisms warrant explicit consideration. Under MCAR (or MAR given A and coarse covariates), labeled and unlabeled pools are exchangeable for $(\theta_A, \theta_{H|a})$; sizable deviations call for stratified labeling or importance weighting under covariate–shift assumptions (Sugiyama et al., 2007). The Bayesian workflow makes such sensitivities transparent: prior–predictive checks flag implausible regions, PPCs detect lack of fit in (A, H) margins, and targeted sensitivity analyses (uniform vs. Jeffreys priors; global vs. stratified thresholds) quantify the robustness of coverage and interval width—key objectives for PPI in label–scarce regimes.

3 Methods

ADNI data statement (required). Data used in this study were obtained from the Alzheimer's Disease Neuroimaging Initiative (ADNI) database (`adni.loni.usc.edu`). ADNI began in 2003 as a public–private partnership led by Michael W. Weiner, MD. Its goals include combining MRI, PET, biofluid biomarkers, and neuropsychological assessments to track progression of MCI and Alzheimer's disease, validating biomarkers for clinical trials, broadening cohort diversity, and providing data to the research community. See `adni.loni.usc.edu` for up-to-date details.

Data version. We downloaded ADNI data on **2025-07-14** and checked for updates prior to submission.

3.1 Generative specification, estimand, and extensions

Let $A \in 0, 1$ denote an autorater decision (derived from a probabilistic score $p \in [0, 1]$ via a fixed operating threshold t) and let $H \in 0, 1$ be a human label. Abundant autorater outputs are observed as $\mathcal{D}_A = A_i * i = 1^{N_A}$ together with a comparatively small labeled subset $\mathcal{D}_H = (A_i, H_i) * i = 1^{N_H}$, with $N_A \gg N_H$. Define

$$\theta_A = P(A = 1), \qquad \theta_{H|1} = P(H = 1 \mid A = 1), \qquad \theta_{H|0} = P(H = 1 \mid A = 0),$$

which determine the population functional

$$g(\boldsymbol{\theta}) = \theta_A \theta_{H|1} + (1 - \theta_A)\theta_{H|0}, \qquad \boldsymbol{\theta} = (\theta_A, \theta_{H|1}, \theta_{H|0}) \in (0, 1)^3. \tag{3.1}$$

We assume $(A_i) * i = 1^{N_A} \overset{\text{i.i.d.}}{\sim} \text{Bernoulli}(\theta_A)$ and, conditionally on A_i, $H_i \mid A_i \overset{\text{ind}}{\sim} \text{Bernoulli}(\theta_{H|A_i})$ for the N_H labeled pairs. Missingness of H is treated as MCAR outside $1, \ldots, N_H$, ensuring exchangeability of labeled and unlabeled pools for inference on $\boldsymbol{\theta}$. Autorater probabilities p_i are thresholded into $A_i = \mathbf{1}p_i \geq t$, where t is regarded as fixed during inference (deployment practice); section 3.4 propagates uncertainty in the selection of t. For a step-by-step summary of how this generative specification is used in practice (from priors and likelihood to posterior summaries of g), see Section J.1.

Likelihood and priors.

Proposition 3.1 (Conjugate posterior for the base chain-rule model)**.** *Let* $n_A = \sum_{i=1}^{N_A} A_i$, $n_{11} = \sum_{i=1}^{N_H} \mathbf{1}\{A_i = 1, H_i = 1\}$, $n_{10} = \sum_{i=1}^{N_H} \mathbf{1}\{A_i = 1, H_i = 0\}$, $n_{01} = \sum_{i=1}^{N_H} \mathbf{1}\{A_i = 0, H_i = 1\}$, $n_{00} = \sum_{i=1}^{N_H} \mathbf{1}\{A_i = 0, H_i = 0\}$. *With independent* $\text{Beta}(\alpha_A, \beta_A)$, $\text{Beta}(\alpha_1, \beta_1)$, $\text{Beta}(\alpha_0, \beta_0)$ *priors, the posterior factorizes as*

$$\theta_A \mid \mathcal{D} \sim \text{Beta}(\alpha_A + n_A,\ \beta_A + N_A - n_A),$$

$$\theta_{H|1} \mid \mathcal{D} \sim \text{Beta}(\alpha_1 + n_{11},\ \beta_1 + n_{10}), \quad \theta_{H|0} \mid \mathcal{D} \sim \text{Beta}(\alpha_0 + n_{01},\ \beta_0 + n_{00}).$$

Thus $g = \theta_A \theta_{H|1} + (1 - \theta_A)\theta_{H|0}$ *follows by direct Monte Carlo.*

Under these assumptions, the complete–data likelihood factorizes as

$$p(\mathcal{D}_A, \mathcal{D}_H \mid \boldsymbol{\theta}) = \prod_{i=1}^{N_A} \theta_A^{A_i}(1 - \theta_A)^{1 - A_i} \prod_{i=1}^{N_H} \theta_{H|1}^{H_i A_i}(1 - \theta_{H|1})^{(1 - H_i)A_i} \theta_{H|0}^{H_i(1 - A_i)}(1 - \theta_{H|0})^{(1 - H_i)(1 - A_i)}. \tag{3.2}$$

Unless stated otherwise, independent Beta$(1,1)$ priors are placed on $(\theta_A, \theta_{H|1}, \theta_{H|0})$; Jeffreys' Beta$(\frac{1}{2}, \frac{1}{2})$ priors are used for sensitivity near the boundaries (Gelman et al., 2013). Weakly informative alternatives (e.g., logit–normal $\theta = \text{logit}^{-1}(\eta)$ with $\eta \sim \mathcal{N}(0, 1.5^2)$) are considered when extreme class imbalance or tiny stratum counts induce separation (Gelman et al., 2008).

Identifiability and small–cell regularization. θ_A is identified from $\mathcal{D}_A$ alone; $(\theta_{H|1}, \theta_{H|0})$ are identified from $\mathcal{D}_H$ provided each stratum $A \in 0, 1$ contributes at least one labeled case asymptotically. When labeled positives (or negatives) are extremely rare in a stratum, Beta priors regularize cell–probability posteriors away from 0/1; posterior predictive checks (PPCs) on the 2×2 table clarify the degree of regularization.

Continuous–score generalization. If one wishes to avoid dichotomizing p, a K–bin chain rule replaces $A \in 0, 1$ by $B \in 1, \ldots, K$ with

$$g = \sum_{k=1}^{K} P(H = 1 \mid B = k)\, P(B = k).$$

and independent Beta priors on $P(H{=}1 \mid B = k)_{k=1}^{K}$ and a Dirichlet prior on $(P(B{=}1), \ldots, P(B{=}K))$. This yields a strictly richer CRE at the cost of more parameters and potentially sparser labeled cells; we therefore default to $K{=}2$ and assess $K > 2$ in sensitivity analyses. Empirically, small multi-bin generalizations ($K \in 4, 5$) using quantile binning produced posterior means of g indistinguishable from $K{=}2$ and 95

Hierarchical partial pooling across strata. For age–aware deployment with strata $s \in 1, \ldots, S$, parameters become $\boldsymbol{\theta}_s = (\theta_{A,s}, \theta_{H|1,s}, \theta_{H|0,s})$ and we impose logit–normal hierarchies $[\ \text{logit}(\theta_{H|a,s}) \sim \mathcal{N}(\mu_a, \sigma_a^2)$, $\text{logit}(\theta_{A,s}) \sim \mathcal{N}(\mu_A, \sigma_A^2),\ ]$ with weakly informative hyperpriors $\mu_\cdot \sim \mathcal{N}(0, 2^2)$ and $\sigma_\cdot \sim$ Half-Normal(1), enabling partial pooling when certain strata have few labels while permitting stratum–specific deviations.

3.2 Bayesian computation, diagnostics, and uncertainty for functionals

Posterior inference targets $p(\boldsymbol{\theta} \mid \mathcal{D}_A, \mathcal{D}_H) \propto p(\mathcal{D}_A, \mathcal{D}_H \mid \boldsymbol{\theta}), p(\boldsymbol{\theta})$. For the base Beta–Bernoulli model, we do not require MCMC: we draw $(\theta_A, \theta_{H|1}, \theta_{H|0})$ directly from their Beta posteriors (Prop. 3.1) and map draws to g. For extensions that break conjugacy (hierarchical logit-normal pooling, non-Beta priors, K-bin with shared hyperparameters, joint t), we use NUTS with the same diagnostics and workflow (Section J.1).

Sampler and parameterization. We use direct Beta sampling in the base conjugate model, and Hamiltonian Monte Carlo with the No–U–Turn Sampler (NUTS) for non-conjugate extensions (Neal, 2011; Hoffman & Gelman, 2014; Betancourt, 2017). Computations are carried out in `PyMC` with automatic differentiation and mass–matrix adaptation (Salvatier et al., 2016; Carpenter et al., 2017). A typical call is

Base (conjugate): direct Beta sampling for $(\theta_A, \theta_{H|1}, \theta_{H|0})$.
Extensions (non-conjugate): `pm.sample(draws=2000, tune=1000, target_accept=0.95, chains=4)`.

with logits $\eta = \text{logit}(\theta)$ as sampling parameters to improve geometry and avoid boundary pathologies. We increase `target_accept` to 0.95 or add non–centered parameterizations in the hierarchical model when divergences occur.

Diagnostics and remedial actions. Convergence is assessed via rank–normalized $\hat{R} < 1.01$, bulk/tail ESS > 400 per parameter, and absence of divergences; energy–Bayes fraction of missing information (E–BFMI) flags poor momentum resampling when < 0.3 (Vehtari et al., 2021b;a). PPCs compare replicated and observed margins of (A, H) and the induced distribution of g; simulation–based calibration (SBC) checks calibration of posteriors across synthetic draws (Gabry et al., 2019; Talts et al., 2018). If PPCs indicate misfit (e.g., skewed residual cell counts), we enlarge priors or move to the hierarchical/continuous–bin extensions above.

Posterior summaries for g and contrasts. For each retained draw $\boldsymbol{\theta}^{(s)}$, compute $g^{(s)}$ via equation 3.1 and report posterior mean, SD, and credible intervals (equal–tailed or highest–density). For strata s, we

propagate to differences $g_s - g_{s'}$ by transforming paired draws; joint intervals for $(g_1, \ldots, g_S)$ use empirical posterior quantiles. When t varies across strata, we re–fit per stratum so uncertainty reflects the induced $(\theta_{H|1,s}, \theta_{H|0,s})$.

Computational cost. The base (non–hierarchical) model has dimension 3 and mixes in milliseconds per iteration; hierarchical variants scale linearly in S,and remain inexpensive for $S \leq 10$. All experiments run comfortably on a laptop CPU.

3.3 Baselines, frequentist connections, and coverage design

We compare against **three** baselines.

(i) Labeled–only Bayes (NB). Model $H_i \overset{\text{iid}}{\sim} \text{Bernoulli}(\theta_H)$ with $\theta_H \sim \text{Beta}(1,1)$, so $g = \theta_H$ has the closed–form posterior

$$\theta_H \mid \{H_i\} \sim \text{Beta}\Big(1 + \sum_i H_i,\ 1 + N_H - \sum_i H_i\Big).$$

(ii) Difference estimator (DE). Define

$$\hat{g}_{\text{diff}} = \bar{A} + \overline{(H - A)} = \frac{1}{N_A}\sum_{i=1}^{N_A} A_i + \frac{1}{N_H}\sum_{i=1}^{N_H}(H_i - A_i),$$

with variance $\text{Var}(\hat{g}_{\text{diff}}) = \text{Var}(A)/N_A + \text{Var}(H - A)/N_H$. Nonparametric bootstrap with $B \in [500, 1000]$ resamples yields percentile CIs (Lohr, 2019; Efron & Tibshirani, 1993).

(iii) Prior-free analytic PPI (continuous p). Using probabilities p_i instead of A_i, let

$$\hat{g}_{\text{PPI}} = \bar{p} + \overline{(H - p)}, \qquad \text{SE}(\hat{g}_{\text{PPI}}) = \sqrt{\widehat{\text{Var}}(p)/N_A + \widehat{\text{Var}}(H - p)/N_H},$$

and form $100(1-\alpha)\%$ intervals with $z_{1-\alpha/2}$ (or $t_{1-\alpha/2,n-1}$ when $n < 30$) (Angelopoulos et al., 2023; Efron & Tibshirani, 1993). This provides a prior–free reference against which CRE's gains can be judged.

Asymptotics and label efficiency. When $N_A \to \infty$ and N_H is fixed, $\bar{A} \to \theta_A$ rapidly while uncertainty is dominated by the labeled rectifier, motivating our Bayesian CRE which borrows strength structurally from $\mathcal{D}_A$. In finite samples, CRE intervals are typically shorter than NB and DE at the same label budget while maintaining coverage, as borne out empirically. *A short theoretical link showing the CRE posterior mean as a first-order shrinkage variant of the DE is provided in App. A.*

Coverage protocol. We evaluate absolute bias, RMSE, average 95% interval width, and empirical coverage over $M = 50$ independent replications with $(\theta^\star_A, \theta^\star_{H|1}, \theta^\star_{H|0}) = (0.6, 0.8, 0.3)$ so that $g_{\text{true}} = 0.60$, and $(N_A, N_H) = (1000, 100)$. Scenarios vary label budgets $n \in 10, 20, 40, 80$, class imbalance, and priors (Uniform vs. Jeffreys). ROC/AUC for probabilities p are reported with nonparametric bootstrap CIs to inform threshold selection and permutation tests for stratified AUC comparisons; these do not enter CRE fitting (Hanley & McNeil, 1982; Fawcett, 2006; Efron & Tibshirani, 1993).

3.4 Operating thresholds, calibration, and propagation of threshold uncertainty

Autorater scores p are mapped to hard decisions $A = \mathbf{1}p \geq t$.

Selection of t (OOF vs. leaky). We study (i) a conventional $t = 0.5$, (ii) Youden's $t^\star_Y \in \arg\max_t \text{TPR}(t) + \text{TNR}(t) - 1$, and (iii) a cost–sensitive Bayes threshold

$$t^\star_{\text{Bayes}} = \frac{C_{10}(1-\pi)}{C_{10}(1-\pi) + C_{01}\pi}.$$

where π is prevalence and C_{01}, C_{10} are false–negative/false–positive costs (Youden, 1950; Fluss et al., 2005). To avoid optimistic bias, we choose data–driven thresholds by K–fold *out–of–fold* (OOF) selection: for each fold, fit the autorater on $K-1$ folds, compute $t_Y^\star$ on the held–out fold only, and pool OOF decisions across folds. We report the gap between OOF and leaky selection as an audit metric.

Propagation into CRE. Given a chosen t (possibly stratum–specific), we re–compute A and re–fit CRE so that posterior uncertainty reflects the $(\theta_{H|1}, \theta_{H|0})$ induced by t. To quantify uncertainty in $t_Y^\star$, we bootstrap the labeled set B times, obtain $t_{Y,b}^\star$, and summarize its spread; optionally, we integrate over t by averaging posteriors across $t_{Y,b}^\star$ (a simple Bayesian bootstrap over cut–points). At very small label budgets the sampling variability of t can dominate; we therefore report the bootstrap dispersion of $t^\star$ and interpret CRE intervals conditionally on the chosen thresholding policy.

Calibration before thresholding. If reliability diagrams and Brier scores indicate miscalibration, we apply (within–stratum) temperature scaling or isotonic regression to produce calibrated $\tilde{p}$, then threshold $\tilde{p}$ at the chosen rule. These monotone mappings preserve ranking and thus AUC, improving decision quality without affecting CRE's form (Brier, 1950; Murphy, 1973; Guo et al., 2017; Zadrozny & Elkan, 2002).

3.5 Case–study pipeline: data curation, autorater, and end–to–end flow

The medical–imaging case study uses ADNI baseline T1–weighted MRI and clinician labels (Mueller et al., 2005; Jack Jr et al., 2008). DICOM→NIfTI conversion uses `dcm2niix`; volumes are loaded with NiBabel (Li et al., 2016; Brett et al., 2020). Preprocessing: center–crop/pad to a brain bounding box, resample to 64^3, per–volume min–max normalize to $[0, 1]$. The autorater is a lightweight 3D CNN (two Conv3D–ReLU–MaxPool blocks, dense head, sigmoid) trained with Adam at 10^{-4}, batch size 2, 5 epochs in PyTorch/`numpy` (Kingma & Ba, 2014; He et al., 2015; Paszke et al., 2019; Harris et al., 2020). Scores p produce A via the selected thresholding policy; CRE is fit on $(\mathcal{D}_A, \mathcal{D}_H)$ globally and by age strata (50–73, 74–79, 80–100). The end-to-end routine we execute in the case study follows Section J.2 for thresholding/calibration and Section J.1 for Bayesian inference.

Robustness to dataset shift and label missingness. If labeled cases differ from the unlabeled pool (covariate shift), MCAR is violated. Practical mitigations include stratified subsampling for labeling, *propensity–overlap* diagnostics (low AUC for a labeled–vs–unlabeled classifier), propensity–weighted PPCs, and hierarchical pooling that absorbs modest shifts (Rosenbaum & Rubin, 1983). When MAR mechanisms are suspected, one can augment CRE with a logistic missingness model for H and perform joint inference; we leave this to future work and rely on design–stage controls plus PPCs in this study. When labeled and unlabeled pools are not exchangeable due to covariate shift, we outline an importance-weighted variant of CRE (IW-CRE) that replaces unweighted cell counts by density-ratio–weighted counts; see Appendix L.

4 Experiments

4.1 Simulation design, SBC calibration, and posterior behavior

We begin with controlled simulations that mirror the generative specification in Section 3. Unless otherwise noted, parameters are fixed at $(\theta_A^\star, \theta_{H|1}^\star, \theta_{H|0}^\star) = (0.6, 0.8, 0.3)$ so that $g_{\text{true}} = 0.60$, and sample sizes are $(N_A, N_H) = (1000, 100)$. For each Monte Carlo replication $m \in 1, \ldots, M$ with $M = 50$, we draw $A_i^{(m)} \overset{\text{i.i.d.}}{\sim} \text{Bernoulli}(\theta_A^\star)$ for $i \le N_A$ and, for the N_H labeled pairs, $H_i^{(m)} \mid A_i^{(m)} \sim \text{Bernoulli}(\theta^\star_{H|A_i^{(m)}})$. We denote the label budget by $n \equiv N_H$ and vary $n \in \{10, 20, 40, 80\}$. Labeled and unlabeled samples are disjoint and i.i.d. from the same data-generating process, ensuring the exchangeability condition required by PPI comparisons. CRE posteriors use direct Beta sampling in the base conjugate model; non-conjugate extensions use `PyMC`+NUTS with `chains=4` and `target_accept=0.95`. Diagnostics are summarized with `ArviZ` (Salvatier et al., 2016; Kumar et al., 2019; Hoffman & Gelman, 2014; Vehtari et al., 2021b). Rank-normalized $\hat{R}$ is < 1.01 for all scalar parameters and derived functionals, bulk/tail ESS exceeds 400, and

no post-warmup divergences are observed, satisfying current best-practice thresholds (Vehtari et al., 2021b; Betancourt, 2017).

Prior-free baselines. Alongside CRE, we evaluate two prior-free baselines: (a) the *probability PPI* using predicted probabilities p, with $\hat{g}_{\text{PPI}} = \bar{p} + \overline{(H - p)}$; and (b) the *difference estimator (DE)* on binary A, $\hat{g}_{\text{diff}} = \bar{A} + \overline{(H - A)}$. Unless otherwise noted, *all* estimators use BCa bootstrap (2,000 resamples) to form 95% CIs (Cochran, 1977; Lohr, 2019). *p-generation*: we set

$$p_i = \min\{\max(\theta^\star_{H|A_i} + \varepsilon_i,\, 10^{-4}),\, 1 - 10^{-4}\}, \qquad \varepsilon_i \sim \mathcal{N}(0, 0.05^2),$$

applied identically to unlabeled and labeled pools. *Design detail*: within each replicate m, when comparing priors (Uniform vs. Jeffreys) we reuse the *same labeled index set*; differences therefore reflect priors rather than re-sampled label sets.

SBC calibration. We validate the engine via Simulation–Based Calibration (SBC): draw $(\theta_A, \theta_{H|1}, \theta_{H|0})$ from the prior, simulate $(\mathcal{D}_A, \mathcal{D}_H)$, fit, and compute posterior ranks for the primitives and the derived g. We use the same (N_A, N_H) and NUTS settings as in the main simulation. Full 2×2 rank–histogram panels and goodness–of–fit p–values appear in Appendix Section I; all panels are visually close to uniform with non–significant χ^2 and KS tests, supporting approximate calibration (Talts et al., 2018; Gabry et al., 2019).

Posterior summaries for g concentrate tightly around $g_{\text{true}} = 0.60$. Across the $M = 50$ datasets, posterior means/medians show negligible bias; medians are slightly less sensitive to occasional skew under the smallest label budgets; see Figure 8. Posterior predictive checks (PPCs) on the 2×2 (A, H) margin and on g display no systematic misfit; the posterior predictive distribution covers the observed margins with tail-area p-values in $[0.22, 0.78]$ (Gelman et al., 2013; Gabry et al., 2019).

DE vs. CRE (simulation) Table 1 summarizes coverage (Cov.) and mean 95% width (W). At very small n (e.g., n=10), PPI attains near-nominal coverage in our runs (Cov. ≈ 0.96) while producing narrower intervals; CRE also achieves near-nominal coverage with slightly wider intervals. As n grows ($n \geq 40$), coverage aligns and CRE often yields the narrowest intervals.

Table 1: Simulation (M=50): empirical 95% coverage (Cov.) and mean interval width (W) for four estimators. PPI is prior-free; CRE/Naïve/Diff are shown under Uniform/Jeffreys.

n_{labels}	Prior	PPI		CRE		Naïve		Diff	
		Cov.	W	Cov.	W	Cov.	W	Cov.	W
10	Uniform	0.960	0.371	1.000	0.382	0.960	0.484	0.560	0.244
10	Jeffreys	0.960	0.371	1.000	0.390	0.940	0.493	0.660	0.308
20	Uniform	0.940	0.245	1.000	0.284	0.980	0.372	0.880	0.261
20	Jeffreys	0.940	0.245	0.980	0.260	0.980	0.380	0.800	0.237
40	Uniform	0.900	0.169	1.000	0.190	0.980	0.276	0.980	0.183
40	Jeffreys	0.900	0.169	1.000	0.184	0.980	0.278	0.960	0.186
80	Uniform	0.900	0.120	0.980	0.137	0.980	0.198	0.940	0.138
80	Jeffreys	0.900	0.120	0.920	0.131	0.940	0.198	0.940	0.133

DE vs. CRE (simulation, 65–70 subset) For completeness, we repeat the coverage/width study on the fixed 65–70 subset. Full plots and the numeric table are deferred to Appendix Section F; see Figure 6 and table 9. **Summary.** Across $n \in \{10, 20, 40, 80\}$, CRE attains near-nominal coverage under both Uniform and Jeffreys priors, with interval widths consistently smaller than Naïve and comparable to (often narrower than) Diff for $n \geq 40$. The prior-free PPI (probability) line is identical across priors and therefore plotted once; qualitative conclusions mirror the full-cohort results.

Stress tests: label scarcity, class imbalance, and prior sensitivity. We vary $n \in \{10, 20, 40, 80\}$ and prevalence $g_{\text{true}} \in \{0.25, 0.40, 0.60\}$ (via $(\theta^\star_A, \theta^\star_{H|1}, \theta^\star_{H|0})$), swapping Uniform vs. Jeffreys priors. In our

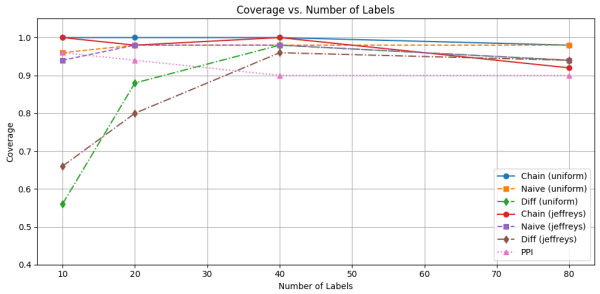

(a) Coverage vs. # labels (PPI, CRE, Naïve, Diff; CRE shown under Uniform/Jeffreys)

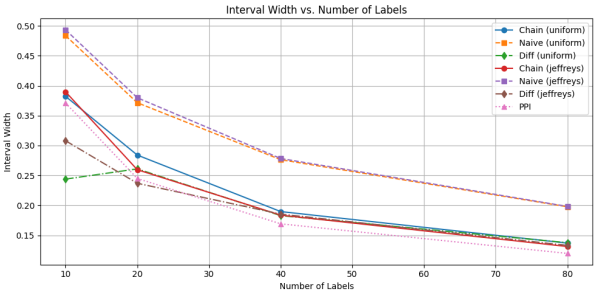

(b) Mean 95% interval width (same four estimators)

Figure 1: Full cohort results for $n \in \{10, 20, 40, 80\}$. PPI is prior-free; CRE uses Uniform/Jeffreys priors.

simulations, CRE *exhibits* near-nominal coverage across conditions; Jeffreys slightly stabilizes coverage at the smallest n when any of $(\theta_{H|1}, \theta_{H|0})$ is near-boundary (e.g., ≥ 0.95), reflecting information-matching behavior (Gelman et al., 2013). For probability-PPI, under-coverage at very small n is driven primarily by CI construction (normal approximation) and by the quality/calibration of p; with BCa bootstrap or better-calibrated p, coverage improves and converges rapidly by $n \geq 40$.

Misspecification checks and benign shift. We probe robustness by allowing the autorater threshold t to drift within a band ($t \in [t_0 - \delta, t_0 + \delta]$ with $\delta \in \{0.02, 0.05\}$) between training and monitoring, and by introducing covariate shift on $P(A{=}1)$ while holding $P(H{=}1 \mid A)$ fixed (Shimodaira, 2000; Sugiyama et al., 2007). Because g depends on both $P(A)$ and $P(H \mid A)$, credible intervals target the distribution of the labeled set unless labeled and unlabeled pools are exchangeable in (A, H) under the operative threshold. When $P(A)$ shifts, we restore exchangeability via stratified CRE or importance weighting; when $P(H{=}1 \mid A)$ also shifts, stratified re-labeling is needed. These adjustments maintain coverage in our ablations, consistent with domain-adaptation intuition (Ben-David et al., 2010).

4.2 ADNI case study: discrimination, thresholds, calibration, and subgroup analysis

We evaluate the MRI autorater on the ADNI cohort (ages 50–100) with the preprocessing and CNN described in Section 3 (Mueller et al., 2005; Jack Jr et al., 2008; Paszke et al., 2019; Harris et al., 2020). Overall ROC and AUC (Fig. 2) use nonparametric bootstrap ($B{=}2000$) (Hanley & McNeil, 1982; Efron & Tibshirani, 1993; Fawcett, 2006). Age-stratified ROCs (Fig. 3) show uniformly strong discrimination with slight attenuation for 80–100; Table 3 reports stratum sizes, prevalence, AUC, and 95% CIs. Pairwise AUC comparisons via two-sided permutation tests show no significant differences; Holm-adjusted p-values are in Table 11.

Operating thresholds per stratum are selected by maximizing Youden's index; $t_Y^\star$ increases with age, trading small TPR drops for larger TNR gains (Table 4) (Youden, 1950; Fluss et al., 2005). We then refit CRE per stratum to propagate the induced $(\theta_{H|1}, \theta_{H|0})$, enabling age-aware monitoring with calibrated intervals.

Probability reliability complements discrimination: Brier scores (50–73: 0.070; 74–79: 0.079; 80–100: 0.106) and reliability diagrams indicate mild underconfidence in the youngest stratum and overconfidence in the oldest. Post-hoc calibration (temperature scaling, isotonic regression) improves probability reliability without altering ranking; AUC remains unchanged while thresholded decisions A better align with clinical preferences (Brier, 1950; Murphy, 1973; Guo et al., 2017; Niculescu-Mizil & Caruana, 2005; Zadrozny & Elkan, 2002). Because CRE consumes only A, it integrates seamlessly with probability-level adjustments.

Prevalence estimation on real data: PPI vs. CRE. On real ADNI data, PPI and CRE estimates of g agree to three decimals overall and by age, with CRE intervals typically narrower; see Table 2.

To probe subgroup equity, we examine dispersion of calibration errors across age strata and re-run CRE after stratum-specific calibration. Multicalibration-style checks (empirical calibration within computationally

Table 2: Prevalence estimates g on ADNI (overall and by age).

Scope	N	PPI $\hat{g}$ [95%]	CRE (Uniform) [95%]	CRE (Jeffreys) [95%]
Overall	2,116	0.308 [0.283, 0.333]	0.308 [0.289, 0.329]	0.308 [0.288, 0.328]
50–73	737	0.343 [0.313, 0.372]	0.332 [0.307, 0.359]	0.332 [0.305, 0.359]
74–79	695	0.310 [0.280, 0.341]	0.306 [0.279, 0.332]	0.306 [0.280, 0.333]
80–100	684	0.268 [0.234, 0.302]	0.292 [0.266, 0.318]	0.291 [0.267, 0.318]

identifiable subgroups) show reduced dispersion after age-wise calibration (Hebert-Johnson et al., 2018; Pleiss et al., 2017).

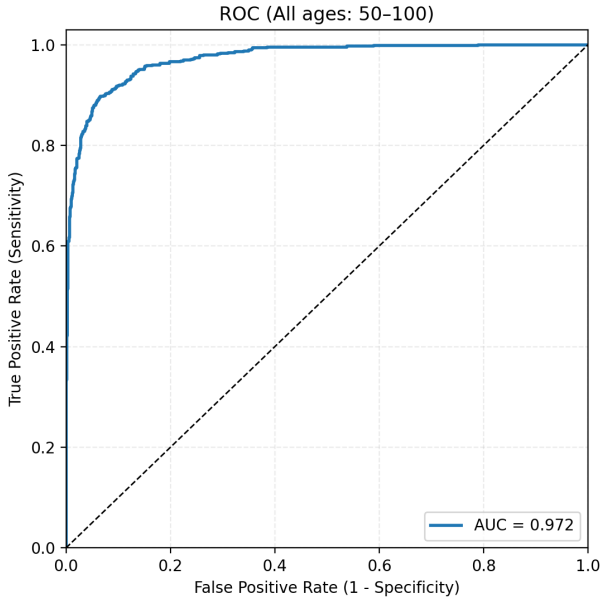

Figure 2: Overall ROC on the full cohort (ages 50–100). Shaded belt: 95% bootstrap band.

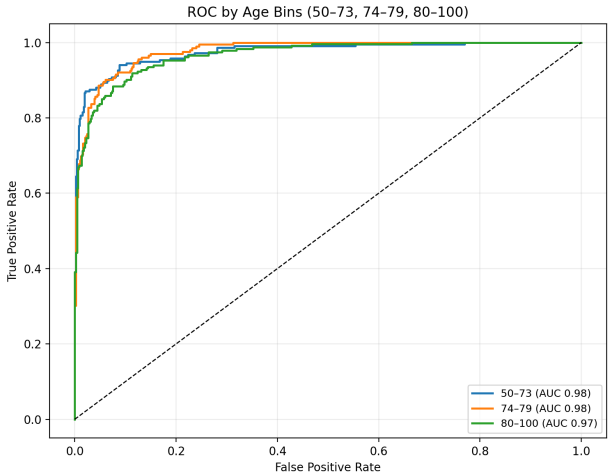

Figure 3: Age–stratified ROC curves with 95% bootstrap bands.

Table 3: Age–stratified discrimination: sample size (n), prevalence, AUC, and 95% bootstrap CIs.

Age bin	n	Prevalence	AUC	95% CI
50–73	737	0.294	0.975	[0.963, 0.986]
74–79	695	0.291	0.977	[0.967, 0.986]
80–100	684	0.341	0.967	[0.953, 0.978]

Table 4: Operating points by age: fixed t=0.5 vs. Youden's $t^\star_Y$. Entries show point estimates with 95% CIs (Wilson), and AUC with 95% bootstrap CI.

Age bin	Threshold	ACC	TPR	TNR	AUC (95% CI)
50–73	$t = 0.5$	0.916 [0.894, 0.934]	0.917 [0.873, 0.947]	0.915 [0.888, 0.936]	0.975 [0.963, 0.986]
50–73	$t^\star_Y = 0.484$	0.920 [0.898, 0.937]	0.940 [0.900, 0.965]	0.912 [0.884, 0.933]	0.975 [0.963, 0.986]
74–79	$t = 0.5$	0.901 [0.876, 0.921]	0.946 [0.905, 0.969]	0.882 [0.851, 0.908]	0.977 [0.967, 0.986]
74–79	$t^\star_Y = 0.586$	0.928 [0.906, 0.945]	0.901 [0.852, 0.935]	0.939 [0.914, 0.957]	0.977 [0.967, 0.986]
80–100	$t = 0.5$	0.858 [0.830, 0.882]	0.953 [0.917, 0.973]	0.809 [0.771, 0.843]	0.967 [0.953, 0.978]
80–100	$t^\star_Y = 0.682$	0.911 [0.887, 0.930]	0.884 [0.837, 0.919]	0.925 [0.896, 0.946]	0.967 [0.953, 0.978]

4.3 Computation, diagnostics, and reproducibility

We report runtime and efficiency for CRE on the full cohort and per-stratum analyses. On a single CPU (12 threads), four NUTS chains with `tune=1000` and `draws=2000` complete within minutes; effective samples per second (bulk ESS/s) exceed 800 for θ_A and > 500 for $(\theta_{H|1}, \theta_{H|0})$. Monte Carlo standard errors (MCSE) for g are $< 10^{-3}$ by batch-means estimates, well below the posterior SD (Flegal & Jones, 2008; Geyer, 2011). We release scripts for data preparation, simulation, model fitting, and figure/table generation to ensure end-to-end reproducibility and independent verification (Carpenter et al., 2017; Salvatier et al., 2016; Kumar et al., 2019; Vehtari et al., 2021a).

Summary. Across synthetic and real-data experiments, CRE delivers (i) calibrated posteriors validated by SBC and PPC; (ii) near-nominal coverage with materially narrower intervals at fixed label budgets compared with labeled-only and prior-free baselines at small/medium n; (iii) robustness under modest threshold drift and covariate shift when labeled/unlabeled pools remain exchangeable for (A, H) or after stratified refits; and (iv) principled uncertainty propagation to age-aware operating points and subgroup-calibrated deployments.

5 Conclusion

We presented a Bayesian realization of prediction–powered inference that uses direct conjugate sampling in the base chain-rule model and NUTS only for non-conjugate extensions. By borrowing strength from abundant autorater outputs while rectifying with a small labeled subset, the chain–rule estimator (CRE) delivered near–nominal coverage with materially narrower intervals than labeled-only and design-based difference baselines, consistent with the core PPI intuition (Angelopoulos et al., 2023) and our empirical evaluations. The approach follows contemporary Bayesian workflow practices (prior/PPC checks, SBC, $\hat{R}$, ESS) and slots naturally into routine monitoring pipelines (Vehtari et al., 2021a; Talts et al., 2018; Hoffman & Gelman, 2014; Betancourt, 2017).

Beyond this, our study adds three practical components that make deployment-time inference more transparent and auditable. First, we include a *prior-free, analytic PPI* baseline—using probabilities p—reported alongside CRE so users can see how much efficiency comes from modeling vs. pure calibration (Cochran, 1977; Deville & Särndal, 1992; Lohr, 2019; Särndal et al., 1992). Second, we explicitly test the *exchangeability* assumption by a labeled–vs–unlabeled propensity AUC (near-0.5 overlap in our data), and we document an *OOF vs. leaky* threshold selection policy with a bootstrap dispersion for the chosen cut-point, then propagate

that threshold uncertainty through CRE. Third, we give a short theoretical link showing the *CRE posterior mean is a first-order shrinkage variant of the difference estimator*, explaining the empirically observed stabilization at small or imbalanced labeled cells (proof in App. A).

Simulations and ADNI results support these claims. On both the full cohort and the 65–70 subset, CRE attains near-nominal coverage with narrower or comparable intervals at a fixed label budget; SBC and PPC indicate well-calibrated posteriors; and K-bin sensitivity shows that modest multi-bin generalizations behave similarly to K=2 under realistic label counts. In the ADNI case study, age-aware operating points tuned by Youden's index improved specificity for older patients without degrading AUC, while lightweight probability calibration reduced Brier loss and left ranking intact; refitting CRE by stratum then yielded calibrated intervals for the age-specific prevalence functional (Youden, 1950; Guo et al., 2017).

Future work targets robustness and scope: hierarchical pooling across finer strata; continuous-score PPI that avoids hard thresholding; importance-weighted CRE for covariate shift or non-MCAR labeling; and tighter links to semiparametric/doubly-robust estimators so validity extends under broader misspecification (Chakrabortty & Cai, 2018; Gronsbell & Cai, 2018; Bang & Robins, 2005; van der Laan & Rose, 2011). We expect these directions to further improve label efficiency and reliability in high-stakes deployments where inference must remain transparent, auditable, and cost-aware.

Acknowledgments

I thank Professor Russell Steele for his supervision and guidance. Data collection and sharing for the Alzheimer's Disease Neuroimaging Initiative (ADNI) is funded by the National Institute on Aging (NIH U19AG024904). Additional past support includes the National Institute of Biomedical Imaging and Bioengineering, the Canadian Institutes of Health Research, and private-sector contributions through the FNIH (e.g., AbbVie; Alzheimer's Association; Biogen; Bristol-Myers Squibb; Eisai; Eli Lilly; F. Hoffmann–La Roche/Genentech; GE Healthcare; Janssen; Johnson & Johnson; Lundbeck; Merck; Novartis; Pfizer; Piramal Imaging; Servier; Takeda; etc.).

References

Anastasios N. Angelopoulos, Stephen Bates, Emmanuel J. Candès, Lihua Lei, and Jing Lei. Prediction-powered inference. *Science*, 382(6669):669–674, 2023. doi: 10.1126/science.adg6862.

Heejung Bang and James M. Robins. Doubly robust estimation in missing data and causal inference models. *Biometrics*, 61(4):962–973, 2005. doi: 10.1111/j.1541-0420.2005.00377.x.

Shai Ben-David, John Blitzer, Koby Crammer, and Fernando Pereira. A theory of learning from different domains. *Machine Learning*, 79(1–2):151–175, 2010.

Michael Betancourt. A conceptual introduction to hamiltonian monte carlo. *arXiv preprint arXiv:1701.02434*, 2017.

Matthew Brett, Michael Hanke, Christopher J. Markiewicz, Paul McCarthy, Marc-Alexandre Côté, Ben Cipollini, Matteo di Oleggio Castello, Satrajit Ghosh, Demian Wassermann, Stephan Gerhard, et al. Nibabel: Neuroimaging in Python, 2020. URL `https://zenodo.org/record/4295521`.

Glenn W. Brier. Verification of forecasts expressed in terms of probability. *Monthly Weather Review*, 78(1): 1–3, 1950.

Bob Carpenter, Andrew Gelman, Matthew D. Hoffman, Daniel Lee, Ben Goodrich, Michael Betancourt, Marcus Brubaker, Jiqiang Guo, Peter Li, and Allen Riddell. Stan: A probabilistic programming language. *Journal of Statistical Software*, 76(1):1–32, 2017. doi: 10.18637/jss.v076.i01.

Gavin C. Cawley and Nicola L. C. Talbot. On over-fitting in model selection and subsequent selection bias in performance evaluation. *Journal of Machine Learning Research*, 11:2079–2107, 2010.

Abhishek Chakrabortty and T. Tony Cai. Efficient and adaptive linear regression in semi-supervised settings. *Journal of the Royal Statistical Society: Series B (Statistical Methodology)*, 80(4):907–938, 2018. doi: 10.1111/rssb.12282.

William G. Cochran. *Sampling Techniques*. Wiley, 3 edition, 1977.

Jean-Claude Deville and Carl-Erik Särndal. Calibration estimators in survey sampling. *Journal of the American Statistical Association*, 87(418):376–382, 1992. doi: 10.1080/01621459.1992.10475217.

Bradley Efron and Robert Tibshirani. *An Introduction to the Bootstrap*. Chapman & Hall/CRC, 1993. ISBN 9780412042317.

Tom Fawcett. An introduction to ROC analysis. *Pattern Recognition Letters*, 27(8):861–874, 2006.

James M. Flegal and Galin L. Jones. Markov chain monte carlo: Can we trust the third significant figure? *Statistical Science*, 23(2):250–260, 2008.

Ronit Fluss, David Faraggi, and Benjamin Reiser. Estimation of the Youden index and its associated cutoff point. *Biometrical Journal*, 47(4):458–472, 2005.

Jonah Gabry, Daniel Simpson, Aki Vehtari, Michael Betancourt, and Andrew Gelman. Visualization in Bayesian workflow. *Journal of the Royal Statistical Society: Series A*, 182(2):389–402, 2019. doi: 10.1111/rssa.12378.

Andrew Gelman, Aleks Jakulin, Maria Grazia Pittau, and Yu-Sung Su. A weakly informative default prior distribution for logistic and other regression models. *The Annals of Applied Statistics*, 2(4):1360–1383, 2008.

Andrew Gelman, John B. Carlin, Hal S. Stern, David B. Dunson, Aki Vehtari, and Donald B. Rubin. *Bayesian Data Analysis*. Chapman and Hall/CRC, 3 edition, 2013. ISBN 9781439840955.

Charles J. Geyer. Introduction to markov chain monte carlo. In *Handbook of Markov Chain Monte Carlo*, pp. 3–48. Chapman & Hall/CRC, 2011.

Jessica L. Gronsbell and T. Tony Cai. Semi-supervised approaches to the estimation of the ROC curve and the area under the curve. *Biometrics*, 74(2):552–562, 2018. doi: 10.1111/biom.12753.

Chuan Guo, Geoff Pleiss, Yu Sun, and Kilian Q. Weinberger. On calibration of modern neural networks. In *Proceedings of the 34th International Conference on Machine Learning (ICML)*, pp. 1321–1330, 2017.

Yue Guo and Lihua Lei. Confidence sets from prediction-powered inference. *Journal of the American Statistical Association*, 2021. doi: 10.1080/01621459.2021.1996374. URL `https://doi.org/10.1080/01621459.2021.1996374`. Published online.

James A. Hanley and Barbara J. McNeil. The meaning and use of the area under a receiver operating characteristic (ROC) curve. *Radiology*, 143(1):29–36, 1982. doi: 10.1148/radiology.143.1.7063747.

Charles R. Harris, K. Jarrod Millman, Stéfan J. van der Walt, Ralf Gommers, Pauli Virtanen, David Cournapeau, Eric Wieser, Julian Taylor, Sebastian Berg, Nathaniel J. Smith, et al. Array programming with NumPy. *Nature*, 585:357–362, 2020. doi: 10.1038/s41586-020-2649-2.

Kaiming He, Xiangyu Zhang, Shaoqing Ren, and Jian Sun. Delving deep into rectifiers: Surpassing human-level performance on ImageNet classification. In *Proceedings of the IEEE International Conference on Computer Vision (ICCV)*, pp. 1026–1034, 2015.

Ursula Hebert-Johnson, Michael P. Kim, Omer Reingold, and Guy N. Rothblum. Multicalibration: Calibration for the (computationally-identifiable) masses. In *Proceedings of the 35th International Conference on Machine Learning (ICML)*, 2018.

Robert A. Hofer, Ryan J. Tibshirani, and Alexander N. Angelopoulos. A Bayesian formulation of prediction-powered inference. arXiv preprint arXiv:2405.06034, 2024. URL `https://arxiv.org/abs/2405.06034`.

Matthew D. Hoffman and Andrew Gelman. The no-u-turn sampler: Adaptively setting path lengths in hamiltonian monte carlo. *Journal of Machine Learning Research*, 15:1593–1623, 2014. URL `https://jmlr.org/papers/v15/hoffman14a.html`.

Clifford R. Jack Jr, Matt A. Bernstein, Nick C. Fox, Paul Thompson, Gene Alexander, Danielle Harvey, Bret Borowski, Paula J. Britson, Jennifer Whitwell, Chadwick Ward, et al. The Alzheimer's disease neuroimaging initiative (ADNI): MRI methods. *Journal of Magnetic Resonance Imaging*, 27(4):685–691, 2008.

Diederik P. Kingma and Jimmy Ba. Adam: A method for stochastic optimization. *arXiv preprint arXiv:1412.6980*, 2014.

Ravin Kumar, Christopher Carroll, Ari Hartikainen, and Osvaldo Martin. Arviz: A unified library for exploratory analysis of Bayesian models in Python. *Journal of Open Source Software*, 4(33):1143, 2019. doi: 10.21105/joss.01143.

Xiangrui Li, Paul S. Morgan, John Ashburner, Stephen M. Smith, and Chris Rorden. The first step for neuroimaging data analysis: DICOM to NIfTI conversion. *Journal of Neuroscience Methods*, 264:47–56, 2016.

Sharon L. Lohr. *Sampling: Design and Analysis*. CRC Press, 2 edition, 2019. ISBN 9780367197117.

Richard McElreath. *Statistical Rethinking: A Bayesian Course with Examples in R and Stan*. Chapman & Hall/CRC, Boca Raton, FL, 2 edition, 2020.

J. G. Moreno-Torres, T. Raeder, R. Alaiz-Rodríguez, N. V. Chawla, and F. Herrera. A unifying view on dataset shift in classification. *Pattern Recognition*, 45(1):521–530, 2012. doi: 10.1016/j.patcog.2011.06.019.

Susanne G. Mueller, Michael W. Weiner, Leon J. Thal, Ronald C. Petersen, Clifford R. Jack, William Jagust, John Q. Trojanowski, Arthur W. Toga, and Laurel Beckett. Ways toward an early diagnosis in Alzheimer's disease: The Alzheimer's disease neuroimaging initiative (ADNI). *Alzheimer's & Dementia*, 1(1):55–66, 2005.

Allan H. Murphy. A new vector partition of the probability score. *Journal of Applied Meteorology*, 12(4): 595–600, 1973.

Radford M. Neal. Mcmc using hamiltonian dynamics. In Steve Brooks, Andrew Gelman, Galin Jones, and Xiao-Li Meng (eds.), *Handbook of Markov Chain Monte Carlo*, pp. 113–162. Chapman and Hall/CRC, 2011. ISBN 9781420079425.

Alexandru Niculescu-Mizil and Rich Caruana. Predicting good probabilities with supervised learning. In *Proceedings of the 22nd International Conference on Machine Learning (ICML)*, pp. 625–632, 2005. doi: 10.1145/1102351.1102430.

Adam Paszke, Sam Gross, Francisco Massa, Adam Lerer, James Bradbury, Gregory Chanan, Trevor Killeen, Zeming Lin, Natalia Gimelshein, Luca Antiga, et al. PyTorch: An imperative style, high-performance deep learning library. In *Advances in Neural Information Processing Systems*, volume 32, 2019.

John Platt. Probabilistic outputs for support vector machines and comparisons to regularized likelihood methods. In *Advances in Large Margin Classifiers*, pp. 61–74. MIT Press, 1999.

Geoff Pleiss, Aditi Raghunathan, Felix Wu, Jon Kleinberg, and Kilian Q. Weinberger. On fairness and calibration. In *Advances in Neural Information Processing Systems*, 2017.

Joaquin Quiñonero-Candela, Masashi Sugiyama, Anton Schwaighofer, and Neil D. Lawrence (eds.). *Dataset Shift in Machine Learning*. MIT Press, 2009.

Paul R. Rosenbaum and Donald B. Rubin. The central role of the propensity score in observational studies for causal effects. *Biometrika*, 70(1):41–55, 1983.

John Salvatier, Thomas V. Wiecki, and Christopher Fonnesbeck. Probabilistic programming in Python using PyMC3. *PeerJ Computer Science*, 2:e55, 2016. doi: 10.7717/peerj-cs.55.

Carl-Erik Särndal, Bengt Swensson, and Jan Wretman. *Model Assisted Survey Sampling*. Springer, 1992.

Hidetoshi Shimodaira. Improving predictive inference under covariate shift by weighting the log-likelihood function. *Journal of Statistical Planning and Inference*, 90(2):227–244, 2000.

Masashi Sugiyama, Matthias Krauledat, and Klaus-Robert Müller. Covariate shift adaptation by importance weighted cross validation. In *JMLR Workshop and Conference Proceedings (PASCAL Workshop on Statistics and Optimization of Clustering Workshop)*, pp. 1–8, 2007.

Sean Talts, Michael Betancourt, Daniel Simpson, Aki Vehtari, and Andrew Gelman. Validating Bayesian inference algorithms with simulation-based calibration. *arXiv:1804.06788*, 2018.

Mark J. van der Laan and Sherri Rose. *Targeted Learning: Causal Inference for Observational and Experimental Data*. Springer, 2011. doi: 10.1007/978-1-4419-9782-1.

Sudhir Varma and Richard Simon. Bias in error estimation when using cross-validation for model selection. *BMC Bioinformatics*, 7:91, 2006.

Aki Vehtari, Andrew Gelman, and Jonah Gabry. Practical Bayesian model evaluation using leave-one-out cross-validation and WAIC. *Statistics and Computing*, 27(5):1413–1432, 2017. doi: 10.1007/s11222-016-9696-4.

Aki Vehtari, Andrew Gelman, Paul-Christian Bürkner, Jonah Gabry, Daniel Simpson, and Stan Development Team. Bayesian workflow. arXiv preprint arXiv:2011.01808, 2021a.

Aki Vehtari, Andrew Gelman, Daniel Simpson, Bob Carpenter, and Paul-Christian Bürkner. Rank-normalization, folding, and localization: An improved $\hat{R}$ for assessing convergence of MCMC. *Bayesian Analysis*, 16(2):667–718, 2021b. doi: 10.1214/20-BA1221.

W. J. Youden. Index for rating diagnostic tests. *Cancer*, 3(1):32–35, 1950.

Bianca Zadrozny and Charles Elkan. Transforming classifier scores into accurate multiclass probability estimates. In *Proceedings of the Eighth ACM SIGKDD International Conference on Knowledge Discovery and Data Mining*, pp. 694–699, 2002. doi: 10.1145/775047.775151.

A Theory snap-in: CRE posterior mean as a first-order shrinkage variant of the difference estimator

Proposition A.1 (Posterior mean as a first-order shrinkage of the difference estimator)**.** *Consider the base Beta–Bernoulli CRE with independent priors* $\theta_A \sim \mathrm{Beta}(\alpha_A, \beta_A)$, $\theta_{H|1} \sim \mathrm{Beta}(\alpha_1, \beta_1)$, $\theta_{H|0} \sim \mathrm{Beta}(\alpha_0, \beta_0)$, *and let* $\hat{\theta}_A = n_A/N_A$, $\hat{\theta}_{H|1} = n_{11}/(n_{11}+n_{10})$, $\hat{\theta}_{H|0} = n_{01}/(n_{01}+n_{00})$. *Define the classical difference estimator* $\hat{g}_{\mathrm{diff}} = \bar{A} + \overline{(H-A)}$. *Then, under exchangeable labeling and* $N_A \gg N_H$,

$$\mathbb{E}[g \mid \mathcal{D}] = \hat{g}_{\mathrm{diff}} + \lambda_A\big(\mathbb{E}[\theta_A \mid \mathcal{D}] - \hat{\theta}_A\big) + \lambda_1\big(\mathbb{E}[\theta_{H|1} \mid \mathcal{D}] - \hat{\theta}_{H|1}\big) + \lambda_0\big(\mathbb{E}[\theta_{H|0} \mid \mathcal{D}] - \hat{\theta}_{H|0}\big) + O_{\mathbb{P}}(N_A^{-1}),$$

where the weights are $\lambda_A = \hat{\theta}_{H|1} - \hat{\theta}_{H|0}$, $\lambda_1 = \hat{\theta}_A$, $\lambda_0 = 1 - \hat{\theta}_A$. *With Jeffreys priors* $\mathrm{Beta}\big(\frac{1}{2}, \frac{1}{2}\big)$, *each* $\mathbb{E}[\theta \mid \mathcal{D}] - \hat{\theta} = O(N^{-1})$, *so the correction is a small, data–adaptive shrinkage that contracts extreme cells and stabilizes interval width near boundaries (Gelman et al., 2013).*

Proof sketch. Write $g(\boldsymbol{\theta}) = \theta_A\theta_{H|1} + (1-\theta_A)\theta_{H|0}$. A first-order delta expansion about $\hat{\boldsymbol{\theta}} = (\hat{\theta}_A, \hat{\theta}_{H|1}, \hat{\theta}_{H|0})$ gives

$$\mathbb{E}[g \mid \mathcal{D}] \approx g(\hat{\boldsymbol{\theta}}) + \nabla g(\hat{\boldsymbol{\theta}})^\top\Big(\mathbb{E}[\boldsymbol{\theta} \mid \mathcal{D}] - \hat{\boldsymbol{\theta}}\Big), \quad \nabla g(\hat{\boldsymbol{\theta}}) = \big(\hat{\theta}_{H|1} - \hat{\theta}_{H|0},\ \hat{\theta}_A,\ 1 - \hat{\theta}_A\big).$$

Under $N_A \gg N_H$ and exchangeability, $g(\hat{\boldsymbol{\theta}})$ is asymptotically equivalent to the design–unbiased difference form $\hat{g}_{\mathrm{diff}}$ up to $O_{\mathbb{P}}(N_A^{-1})$ terms (linearization and the independence of the large-N_A and labeled components), matching classical calibration/difference–estimator theory (Cochran, 1977; Särndal et al., 1992; Lohr, 2019). Beta posteriors yield $\mathbb{E}[\theta_A \mid \mathcal{D}] = (\alpha_A + n_A)/(\alpha_A + \beta_A + N_A)$ and similarly for $\theta_{H|a}$; substituting gives the stated shrinkage correction. □

Remark (stability near the boundaries). When some (2×2) cells are tiny, Jeffreys or weakly-informative priors keep posterior means away from 0,1, tightening the tail behavior of (g) and making the $(O(N^{-1}))$ correction beneficial in practice (Gelman et al., 2013).

B Prior-free PPI baseline (analytic): estimator and CIs

For the prevalence functional, the *prediction–powered* estimator using probabilities is

$$\hat{g}_{\mathrm{PPI}} = \bar{p} + \overline{(H-p)} = \frac{1}{N_A}\sum_{i=1}^{N_A} p_i + \frac{1}{N_H}\sum_{i=1}^{N_H}(H_i - p_i).$$

with large-sample variance $\widehat{\mathrm{Var}}(\hat{g}_{\mathrm{PPI}}) = \widehat{\mathrm{Var}}(p)/N_A + \widehat{\mathrm{Var}}(H-p)/N_H)$. For very small n we use a t-critical value with Satterthwaite's degrees of freedom; otherwise $z_{0.975}$ suffices. **This is distinct from the *difference estimator* based on binary** A, $\hat{g}_{\mathrm{diff}} = \bar{A} + \overline{(H-A)}$, for which we report nonparametric bootstrap percentile CIs (see Methods).

C Exchangeability diagnostics (propensity overlap)

We train a simple "labeled vs. unlabeled" propensity model and report AUC (near 0.5 implies overlap).

Table 5: Propensity AUC and sample sizes (exchangeability check).

R	n_{labeled}	N	AUC (mean)	95% CI
50	634	2,116	0.522	[0.507, 0.543]

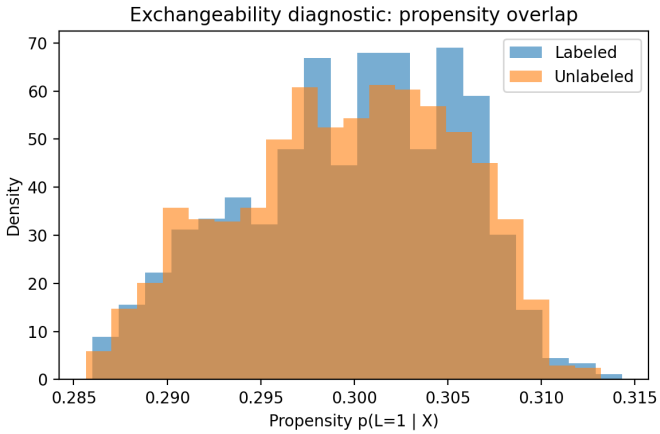

Figure 4: Propensity overlap histograms for labeled vs. unlabeled pools (near-complete overlap).

D Threshold selection: OOF vs. leaky and bootstrap dispersion

OOF vs. leaky (train=eval) selection

Table 6: Five-fold OOF thresholds and performance.

Fold	t_{train}	ACC	TPR	TNR
1	0.6026	0.9151	0.8678	0.9340
2	0.6073	0.9243	0.8790	0.9431
3	0.6026	0.9220	0.8944	0.9359
4	0.6026	0.9173	0.8872	0.9310
5	0.6122	0.9291	0.9318	0.9278

Table 7: Leaky (train=eval) selection

Fold	t_{train}	ACC	TPR	TNR
leaky_full	0.6026	0.9230	0.8972	0.9344

Bootstrap dispersion of Youden thresholds

Table 8: Bootstrap summary of $t^{\star}_{Y}$ and induced metrics.

mean(t)	t_{lo}	t_{hi}	ACC_m	ACC_ℓ	ACC_h	TPR_m	TPR_ℓ	TPR_h	TNR_m	TNR_ℓ	TNR_h
0.601	0.503	0.631	0.921	0.894	0.926	0.896	0.876	0.936	0.933	0.876	0.947

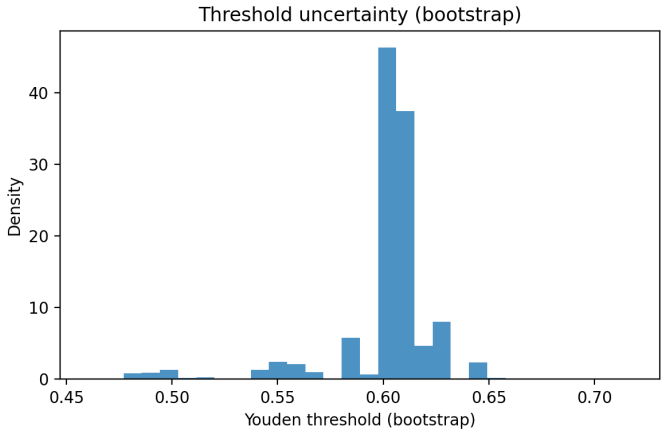

Figure 5: Bootstrap distribution of $t_Y^\star$ and operating metrics.

E DE and PPI baselines: additional simulation tables

Detailed DE vs. CRE numbers are reported in the main text (Table 1); extended tables and per-replication summaries are included in the repository.

F Additional results: Age 65–70 subset

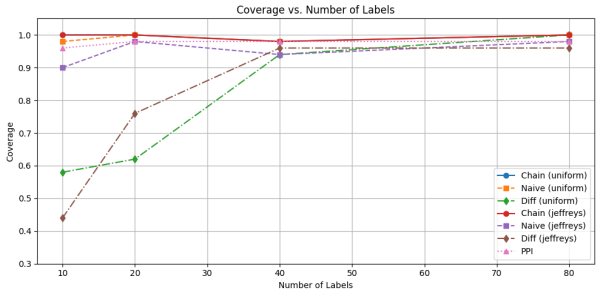

(a) Coverage vs. # labels (65–70; PPI prior-free; CRE under Uniform/Jeffreys)

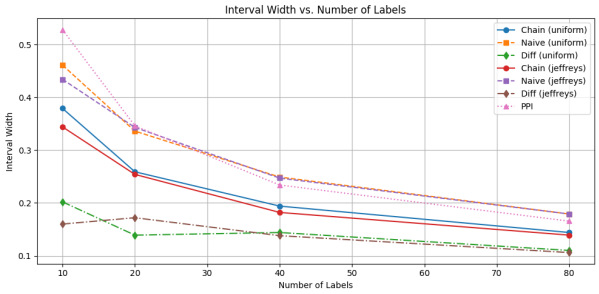

(b) Mean 95% interval width (same estimators)

Figure 6: 65–70 subset: coverage and width across $n \in \{10, 20, 40, 80\}$.

Table 9: 65–70 subset: empirical 95% coverage (Cov.) and mean interval width (W). PPI is prior-free and listed once. CRE/Naïve/Diff are shown under Uniform/Jeffreys.

n_{labels}	Prior	PPI (prob.)		CRE		Naïve		Diff	
		Cov.	W	Cov.	W	Cov.	W	Cov.	W
10	Uniform	0.96	0.528	1.00	0.379	0.98	0.461	0.58	0.202
20	Uniform	0.98	0.346	1.00	0.259	1.00	0.336	0.62	0.139
40	Uniform	0.98	0.234	0.98	0.194	0.98	0.249	0.94	0.144
80	Uniform	0.98	0.166	1.00	0.144	1.00	0.179	1.00	0.110
10	Jeffreys	0.96	0.528	1.00	0.344	0.90	0.434	0.44	0.160
20	Jeffreys	0.98	0.346	1.00	0.254	0.98	0.343	0.76	0.172
40	Jeffreys	0.98	0.234	0.98	0.182	0.94	0.247	0.96	0.138
80	Jeffreys	0.98	0.166	1.00	0.139	0.98	0.179	0.96	0.106

G Prevalence estimates on real data (overall and by age)

Extended versions of Table 2 (stratifications and alternative thresholds) are available in the repository; we keep a single summary table in the main text to avoid duplication.

H K-bin sensitivity (quantile binning)

We compare $K \in 2, 4, 5$ with Dirichlet prior on $(P(B{=}k))$ and Beta priors on $P(H{=}1 \mid B{=}k)$. Under the label budgets considered, increasing K does not materially change $\hat{g}$; CI widths change minimally.

Table 10: K-bin sensitivity summary (numbers generated by repo scripts).

Prior	K	ΔMean vs $K{=}2$	Width ratio ($K/2$)
Uniform	4	-8.55×10^{-5}	1.009
Uniform	5	3.46×10^{-4}	1.001
Jeffreys	4	-7.25×10^{-5}	0.990
Jeffreys	5	1.07×10^{-4}	0.990

Protocol. We fix labeled indices across priors (prior-invariant comparison), use quantile binning with minimal tie drops, and report Δmean and width ratios.

I SBC and additional diagnostics

Over $M_{\text{SBC}} = 500$, posterior rank histograms for $\theta_A, \theta_{H|1}, \theta_{H|0}$ and the derived g are visually close to uniform. With $B = 20$ bins (expected count $= M/B = 25$), fluctuations fall within the nominal 95% binomial band $\approx [15, 35]$. Goodness–of–fit tests are non–significant for all parameters (per–panel p–values in captions), supporting approximate calibration.

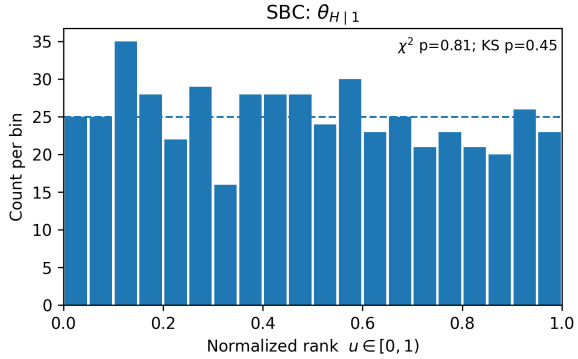

(a) $\theta_{H|1}$: $\chi^2\, p = 0.81$; KS $p = 0.45$

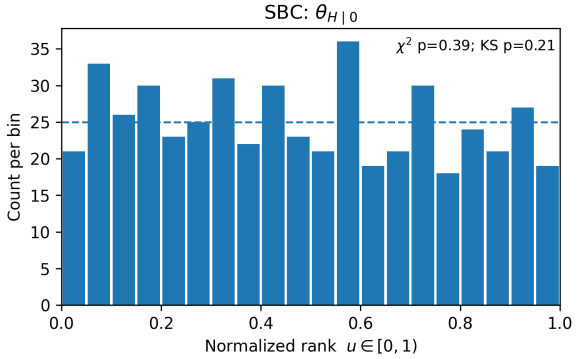

(b) $\theta_{H|0}$: $\chi^2\, p = 0.39$; KS $p = 0.21$

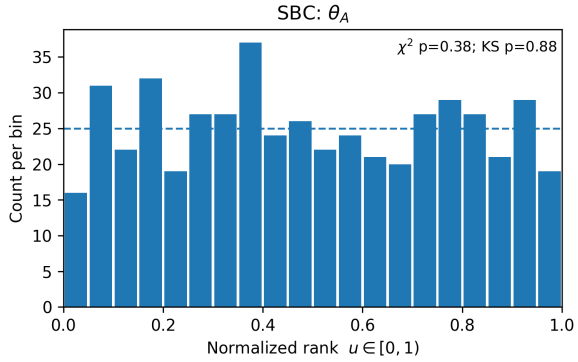

(c) θ_A: $\chi^2\, p = 0.38$; KS $p = 0.88$

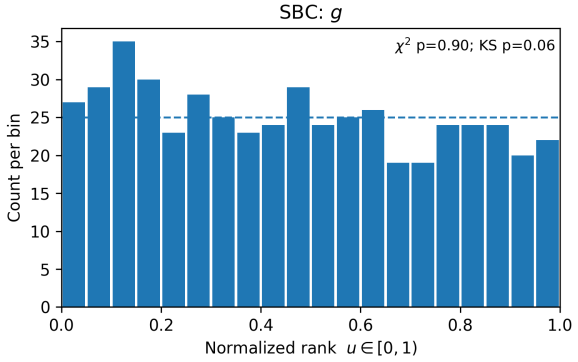

(d) $g = \theta_A\theta_{H|1} + (1-\theta_A)\theta_{H|0}$: $\chi^2\, p = 0.90$; KS $p = 0.06$

Figure 7: SBC rank histograms (M=500, B=20). Dashed line marks the expected per–bin count (25). Counts fluctuate within $[15, 35]$, consistent with binomial variability; tests do not reject uniformity.

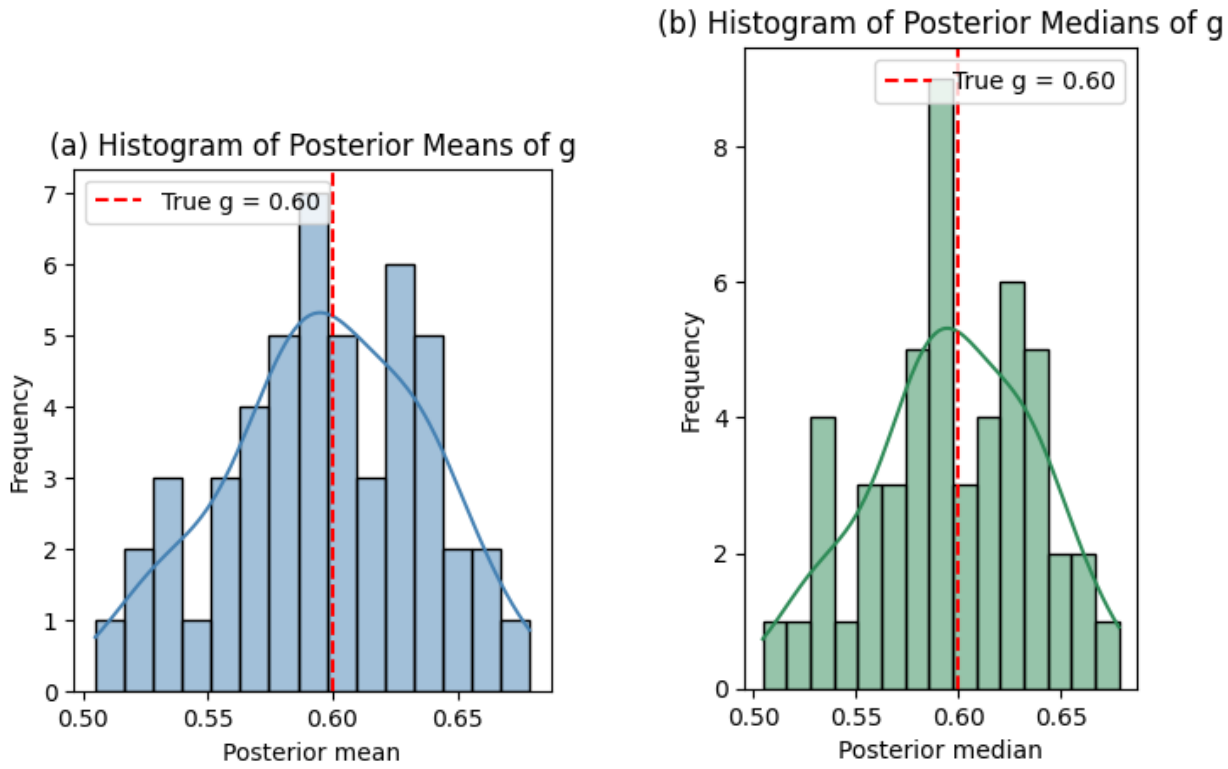

(a) Posterior means across M=50 datasets.

(b) Posterior medians across M=50 datasets.

Figure 8: Posterior mean/median summaries across $M = 50$ replicates (vertical line: $g_{\text{true}} = 0.60$).

J Algorithms (pseudocode)

J.1 Bayesian CRE inference

Algorithm 1 CRE (base: conjugate; extensions: NUTS)

Require: $\mathcal{D}_A = \{A_i\}_{i=1}^{N_A}$, $\mathcal{D}_H = \{(A_i, H_i)\}_{i=1}^{N_H}$, priors
1: Compute cell counts $(n_A, n_{11}, n_{10}, n_{01}, n_{00})$
2: **if** base Beta–Bernoulli **then**
3: Draw $\theta_A, \theta_{H|1}, \theta_{H|0}$ from Beta posteriors (Prop. 1)
4: Map draws to $g = \theta_A\theta_{H|1} + (1-\theta_A)\theta_{H|0}$
5: **else** ▷ hierarchy / non-Beta priors / K-bin / joint t
6: Run NUTS: `draws=2000, tune=1000, target_accept=0.95, chains=4`
7: Check $\hat{R} < 1.01$, bulk/tail ESS, divergences; then map draws to g
8: **end if**
9: PPCs on (A, H) margins and g; optionally SBC for end-to-end checks

J.2 Operating threshold selection and uncertainty propagation

Algorithm 2 Thresholding and calibration workflow

Require: Scores p_i, labels H_i (dev split), policy $\in t{=}0.5, , t^\star_Y, , t^\star_{\text{Bayes}}$
1: **if** $t^\star_Y$ **then**
2: Sweep t; pick t maximizing $J(t) = \text{TPR}(t) + \text{TNR}(t) - 1$
3: Bootstrap labeled set B times to obtain $t^\star_{Y,b}$ and summarize
4: **end if**
5: Calibrate (temperature scaling or isotonic) if needed; apply t to get A
6: Fit CRE on $(\mathcal{D}_A, \mathcal{D}_H)$; report posterior for g (and by strata)

K Permutation tests: age-stratum AUC comparisons

Holm-adjusted p-values (two-sided permutation with label shuffles, bin sizes fixed). No comparison is significant at $\alpha = 0.05$.

Table 11: Pairwise AUC differences across age strata.

Comparison	AUC diff	Adj. p
50–73 vs. 74–79	-0.002190	0.779
50–73 vs. 80–100	0.008512	0.654
74–79 vs. 80–100	0.010702	0.496

L Importance-weighted CRE under covariate shift

Suppose unlabeled data follow $p_{\text{pop}}(X)$ while labels come from $p_{\text{lab}}(X)$. Let stabilized importance weights ($w(x) \propto p_{\text{pop}}(x)/p_{\text{lab}}(x)$), and normalized $\tilde{w}_i = w(X_i)/\big(\frac{1}{n}\sum_j w(X_j)\big)$. Replace unweighted (A, H) margins by their weighted analogs; for the unlabeled pool use $\tilde{v}_i$ analogously. Kish effective sizes ($n^{(H)}_{\text{eff}} = \big(\sum_i \tilde{w}_i\big)^2 / \sum_i \tilde{w}_i^2$), ($N^{(A)}_{\text{eff}} = \big(\sum_i \tilde{v}_i\big)^2 / \sum_i \tilde{v}_i^2$) quantify variance inflation. Conjugate updates proceed with fractional counts:

$$\theta_A \,|\, \mathcal{D} \sim \text{Beta}\big(\alpha_A{+}\tilde{n}_A,\ \beta_A{+}\tilde{N}_A{-}\tilde{n}_A\big),\ \theta_{H|1} \,|\, \mathcal{D} \sim \text{Beta}\big(\alpha_1{+}\tilde{n}_{11},\ \beta_1{+}\tilde{n}_{10}\big),\ \theta_{H|0} \,|\, \mathcal{D} \sim \text{Beta}\big(\alpha_0{+}\tilde{n}_{01},\ \beta_0{+}\tilde{n}_{00}\big).$$

Map draws to g as usual. In practice, clip extreme weights and report n_{eff}.

M Reproducibility checklist

- Seeds fixed (`numpy/PyMC/python`); versions pinned in `environment.yml`.
- Config-driven runs; figures/tables built via `scripts/` and Makefile targets.
- Diagnostics reported: rank-normalized $\hat{R}$, bulk/tail ESS, divergences, E–BFMI.
- SBC: $M_{\mathrm{SBC}} = 500$ with rank histograms.
- Data splits, bootstrap/permutation indices saved and versioned.

N Code and data availability

The full repository, including `src/`, `scripts/`, and `configs/` used for all figures and tables, is available at `(anonymizedlinkorOpenReviewartifactlink)`. ADNI participant-level data cannot be redistributed under the ADNI Data Use Agreement; qualified researchers can apply at `adni.loni.usc.edu`. We release code and summary-level results only.